THE JOURNAL OF PHYSICAL CHEMISTRY C

Article

Cite This: J. Phys. Chem. C XXXX, XXX, XXX−XXX

pubs.acs.org/JPCC

Monolayer, Bilayer, and Heterostructures of Green Phosphorene for Water Splitting and Photovoltaics

Sumandeep Kaur,[†,‡] Ashok Kumar,[*,‡] Sunita Srivastava,[*,†,§] K. Tankeshwar,[*,†,§] and Ravindra Pandey[∥]

[†]Department of Physics, Panjab University, Chandigarh 160014, India

[‡]Department of Physical Sciences, School of Basic and Applied Sciences, Central University of Punjab, Bathinda 151001, India

[§]Department of Physics, Guru Jambheshwar University of Science and Technology, Hisar, Haryana 125001, India

[∥]Department of Physics, Michigan Technological University, Houghton, Michigan 49931, United States

Supporting Information

ABSTRACT: We report the results of density functional theory-based calculations on monolayer and bilayer green phosphorene and their heterostructures with $MoSe_2$. Both monolayer and bilayer green phosphorene are direct band gap semiconductors and possess anisotropic carrier mobility as high as 10^4 $cm^2/V/s$. In bilayers, the pressure of about 9 GPa induces the semiconductor−metal transition. Moreover, the band gap depends strongly on the thickness of the films and the external electric field. By employing strain engineering under suitable solution conditions, monolayer and AC-stacked bilayer green phosphorene offer the band edge alignments which can be used for water splitting. The upper limit of the power conversion efficiencies for monolayer and AB- and AC-stacked bilayer green phosphorene heterostructures with $MoSe_2$ is calculated to be 18−21%. Our results show the possibility of green phosphorene to be used as a photocatalytic and photovoltaic material in energy-related applications.

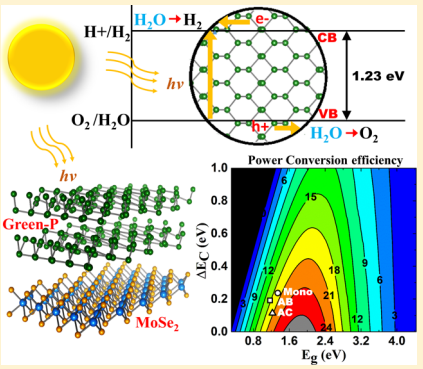

1. INTRODUCTION

After the successful realization of freestanding black phosphorene,[1,2] there exists growing interest among scientific community to explore about its isostructural allotropes. Compared to the previously known two-dimensional (2D) materials, phosphorene shows great potential to be used in practical applications because of its unique properties[3−8] viz. structural anisotropy, high carrier mobility ($\sim 10^3$ $cm^2/V/s$), high lateral flexibility, and tunability of its band gap with number of layers, stacking pattern, electric field, and strain. Because of the inequivalent sp^3 orbital hybridization in its structure, phosphorous in its bulk form is known to exhibit various allotropes like red, white, violet, and black.[3] Since 2014, various allotropes of phosphorene consisting of honeycomb structures (α-, β-, γ-, δ-, and red-phosphorene) and nonhoneycomb structures (ε-, ς-, η-, θ-, octa-, hexstar-, and ψ-phosphorene) have been predicted.[9−17] All of these allotropes are semiconducting with band gap ranging from 0.48 eV for ε-phosphorene to 2.09 eV for octa-phosphorene.[17] Out of all these allotropes, only α- and β-phosphorene have been experimentally realized.[18−21]

The very recently predicted allotrope of phosphorene is green phosphorene[22,23] which is constructed from black phosphorene by flipping every 12th row of bonds upside down followed by the dislocation of armchair ridges after every 4th row. Green phosphorene possesses the monoclinic C_2/m structure with six atoms per unit cell. It shows strong anisotropy in its transport and optical properties. It has been predicted to be more stable than β-P and can be formed from α-P at temperatures above 87 K. Also, it is predicted to be synthesized on corrugated metal substrates.[22]

Motivated by the recent study on green phosphorene, we have investigated bilayer green phosphorene in two types of stacking patterns by applying perpendicular electric field, vertical pressure, and in-plane uniaxial and biaxial strain. By employing the deformation potential (DP) theory, the carrier mobilities of the monolayers and bilayers are investigated. The possibility of strain-engineered monolayer and bilayer green phosphorene to be used for water splitting photocatalytic application has been explored. From application point of view, we combine the monolayer and bilayers of green phosphorene with $MoSe_2$ to form heterostructures which come out to be an appropriate combination to be used as a solar cell. The calculated upper limits to the power conversion efficiencies (PCEs) of heterostructure systems are found to be comparable to the black phosphorene/MoS_2-based heterostructures.[24,25]

2. COMPUTATIONAL DETAILS

SIESTA simulation package has been employed to perform all calculations.[26] Norm-conserving Troullier Martin pseudopotential in fully separable Kleinman and Bylander form is used to treat the electron−ion interactions.[27] The exchange and

Received: September 2, 2018
Revised: October 23, 2018

DOI: 10.1021/acs.jpcc.8b08566
J. Phys. Chem. C XXXX, XXX, XXX−XXX

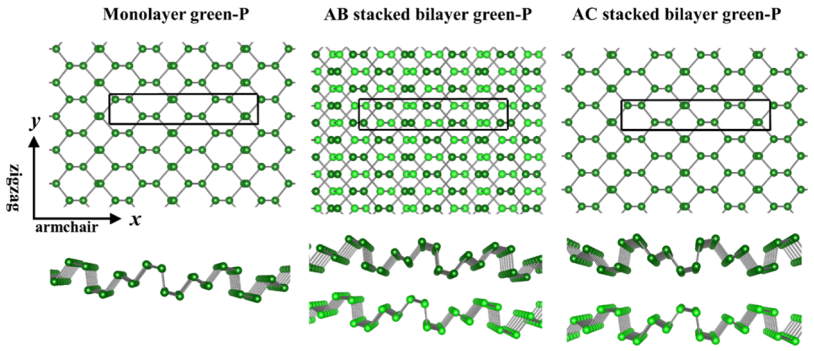

Figure 1. Top and side views of structures of monolayer green phosphorene, AB-stacked bilayer and AC-stacked bilayer green phosphorene. The rectangular box represents the unit cell.

correlation energies are treated within the van der Waals (vdW)-DRSLL functional.[28] The Kohn–Sham orbitals were expanded as a linear combination of numerical pseudoatomic orbitals using a split-valence double zeta basis set with polarization functions (DZP). Throughout geometry optimization, the confinement energy of numerical pseudoatomic orbitals is taken as 0.01 Ry. Minimization of energy was carried out using the standard conjugate-gradient technique. The structures were relaxed until the forces on each atom were less than 0.01 eV/Å. Monkhorst–Pack scheme is used to sample the Brillouin zone with a 30 × 30 × 1 mesh for all of the structures. The spacing of the real space used to calculate the Hartree exchange and correlation contribution of the total energy was 450 Ry. A vacuum region of about 20 Å perpendicular to the 2D plane is used in calculations to prevent the superficial interactions between the periodic images.

3. RESULTS AND DISCUSSIONS

3.1. Monolayer and Bilayer Green Phosphorene. Bulk green phosphorus exists in the monoclinic structure with the space group $C2/m$. The calculated optimized lattice parameters are a = 10.93 Å, b = 3.34 Å, c = 8.26 Å, α = 90.00°, β = 56.36°, and γ = 90.00° [Figure S1], which are in very good agreement with the previously reported values.[22] The calculated direct band gap is 0.32 eV at the GGA-PBE level of theory. Note that the calculated G_0W_0 quasi-particle band gap is 0.68 eV.[22] This dissimilarity in the band gap value is due to the well-known fact that GGA underestimates the band gaps of the materials. To describe interlayer vdW interactions correctly, we include vdw-DRSLL functional for the calculations of multilayer systems.

3.2. Structures and Energetics. It has been established that AB stacking is energetically preferred in 2D materials. In bilayer black phosphorene, AB stacking is the most favorable followed by AC and AA stacking.[24] This is also the case with green phosphorene for which AB stacking is preferred over AA stacking. Therefore, we have considered two most energetically preferred stacking patterns in our study. Figures 1 and S2 illustrate the structures of the monolayer and AB- and AC-stacked bilayers of green phosphorene in the rectangular unit cells. AB-stacking is formed by shifting one of the two layers by half the cell either along x or y direction. For AC-stacking, one of the layers is a mirror image of the other layer. The in-plane and out-of-plane bond lengths in monolayer green phosphorene are not affected much when bilayers are formed. The interlayer distances of AB- and AC-stacked bilayer green phosphorene are calculated to be 3.10 and 3.75 Å, respectively [Table 1].

Table 1. Green Phosphorene: Lattice Constant (a, b), Number of Atoms per Unit Cell (N), Cohesive Energy (E_C), and Elastic Modulus (C) of Monolayer and AB- and AC-Stacked Bilayer Green-P[a]

systems	monolayer	AB-stacked bilayer	AC-stacked bilayer
a, b (Å)	14.83, 3.42	14.87, 3.42	14.89, 3.42
E_C (eV/atom)	4.97	5.00	5.02
no. of atoms	12	24	24
C_{x_2D} (N/m)	26.5	54.5	53.6
C_{y_2D} (N/m)	84.9	168.5	170.9
d (Å)		3.14	3.75
E_B (eV/atom)		0.52	0.26

[a]The interlayer distance (d) and binding energy (E_B) of bilayers is also given.

To determine the energetic stability, we calculate the cohesive energy which is defined as the amount of energy required to break the monolayer or bilayer green phosphorene into isolated single phosphorous atoms, that is, $E_C = \frac{E_A - NE_s}{N}$, where E_A is the total energy of the considered monolayer or bilayer green phosphorene, E_s is the energy of the isolated single phosphorous atom, and N is the number of atoms per unit cell of the monolayer or bilayer green phosphorene. The calculated cohesive energy (4.97 eV/atom) of green phosphorene is nearly equal to that of black phosphorene (4.98 eV/atom) which indicates nearly equal stability of both monolayers. The cohesive energies of AB- and AC-bilayers are calculated to be 5.00 and 5.02 eV/atom, respectively, which depicts the bilayer systems to be energetically more favorable. Also, small binding energy values [Table 1] of the bilayers suggest that weak vdW forces act between the layers. Note that the binding energy is calculated as $E_B = \frac{E_A - (E_1 + E_2)}{N}$, where E_A is the total energy of bilayer green phosphorene, E_1 and E_2 are the energies of the individual layers of the bilayer system within the cell of the bilayer, and N is the number of atoms per unit cell of bilayer green phosphorene.

3.3. Mechanical Properties. To investigate the mechanical stability of the considered mono- and bilayer systems, we calculate the ultimate tensile strength (UTSH) and strain by the calculating strain–stress relationship which can be obtained by calculating the components of the stress tensor with respect to the strain tensor.[9] Here, the stress tensor is a

DOI: 10.1021/acs.jpcc.8b08566
J. Phys. Chem. C XXXX, XXX, XXX–XXX

positive derivative of the total energy with respect to the strain tensor. UTSH is referred to the maximum stress that a layer can withstand before breaking. The point where the slope of the strain−stress curve becomes zero gives the value of UTSH, and the maximum strain at this point represents the magnitude of ultimate tensile strain (UTSR).

Monolayer and AB-stacked bilayer and AC-stacked bilayer green-P can withstand UTSR of up to 30% (20%), 26% (20%), and 30% (20%) along the armchair (zigzag) direction, respectively, with the corresponding UTSH of 2.21 GPa (3.63 GPa), 3.70 GPa (6.65 GPa), and 3.68 GPa (6.13 GPa)[Figure 2a]. The UTSR values for the monolayer and

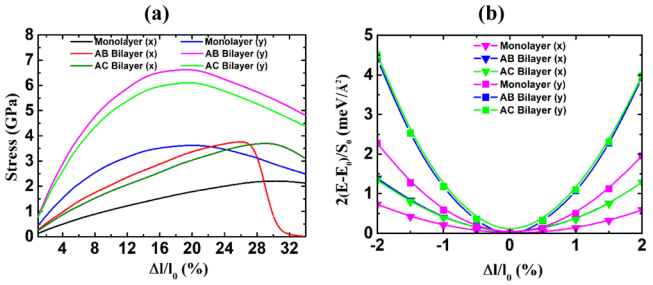

Figure 2. (a) Strain−stress curves and (b) strain vs strain energy density curve for monolayer and AB- and AC-stacked bilayer of green phosphorene.

AC-stacked bilayer green-P are the same. However, the corresponding degree of stress that these layers can withstand at the UTSR value suggests the monolayer to be relatively flexible. Yang et al., have also predicted a higher UTSR in monolayer green phosphorene along the armchair direction as compared to the zigzag direction.[23] The calculated values of UTSR for monolayer green-P are comparable with monolayer black-P (30% along armchair and 27% along zigzag),[32] monolayer MoS_2 (24%), monolayer $MoSe_2$ (26%), and monolayer $MoTe_2$ (28%),[33] whereas they are much higher compared to monolayer blue phosphorene (16%).[34]

To get additional insight into the mechanical stability, we calculate the elastic modulus by applying strain ranging from −2 to +2% in steps of 0.5% along x or y direction and quadratic fitting of eq 3. Figure 2b shows the strain energy density curve for monolayer and AB-stacked bilayer and AC-stacked bilayer green phosphorene. It can be seen that for both monolayer and bilayer green-P, the energy density along x direction is always lower than that along y direction which depicts the highly anisotropic nature of mono- and bilayer green phosphorene. The magnitude of the stiffness, however, increases as we move from monolayer to bilayer [Table 2]. Also, the flexibility of the layers is higher along the armchair direction compared to the zigzag direction owing to a low value of in-plane stiffness along the armchair direction compared to the zigzag direction [Table 2], which is in line with the values reported for other allotropes of phosphorene such as monolayer black-P (24.3 N/m along armchair and 103.3 N/m along zigzag direction) and tricycle-type phosphorene (12.4 N/m along armchair and 89.1 N/m along zigzag direction).[7,14]

3.4. Effect of Thickness, Electric Field, and Pressure on Band Gap. Monolayer green-P is a semiconductor with a direct band gap of ∼1.35 eV. The direct nature of the band gap is preserved on moving from monolayer to bilayer, but the magnitude of band gap decreases to 1.17 and 1.23 eV for the

Table 2. Electron and Hole Effective Mass (m^*), DP (E_1), and Carrier Mobility (μ) of Monolayer Green-P and AB- and AC-Stacked Bilayer Green-P Along the Armchair and Zigzag directions

systems	m^* (x) (m_e)	m^* (y) (m_e)	E_{1x}	E_{1y}	μ (x) cm^2/V/s	μ (y) cm^2/V/s
monolayer (e)	0.27	0.20	−5.02	2.35	355	7020
monolayer (h)	0.21	1.71	−9.93	7.71	48	24
AB bilayer (e)	0.3	0.25	1.47	−4.26	7226	3166
AB bilayer (h)	0.23	1.96	−2.17	−1.12	1589	2179
AC bilayer (e)	0.27	0.21	4.04	−1.01	1104	71 152
AC bilayer (h)	0.23	1.83	−0.77	4.01	13159	192

AB-stacked and AC-stacked bilayer, respectively. The band gaps of ABAB...-type and ACAC...-type stacked layers show a decreasing trend with increase in thickness of the films because of the quantum confinement effect of the charge carriers. These results are in agreement with the other 2D materials such as black phosphorene and MoS_2 [Figure 3a]. For ABAB...-type stacking, the band gap shows direct to indirect transition on moving from $N = 3$ to $N = 4$ and again a transition from indirect to direct band gap at $N = 7$. Similarly, for ACAC... stacking, a direct to indirect band gap transition occurs on moving from $N = 5$ to $N = 6$.

It is well known that electric field and pressure can effectively tune the electronic properties of 2D materials.[35,36] On applying a perpendicular electric field in bilayer green phosphorene, a systematic shift in both valence band maximum (VBM) and conduction band minimum (CBM) has been found [Figure 3b]. At a critical value of field, that is, ±1.0 and ±1.2 V/Å for AB- and AC-stacked bilayers, respectively, band gap closure occurs which may be attributed to the electric field-induced charge redistribution in the vdW gap in bilayers. On applying vertical pressure, metallization occurs for AB- and AC-stacked bilayers at 9 and 8 GPa, respectively [Figure 3c], which is feasible in the real experimental situation. In general, application of pressure via decreasing the interlayer distance in a bilayer facilitates a higher degree of electron hopping which, in general, can lead to semiconductor−metal transition in the lattice. Note that pressure on the bilayer system is calculated as the energy per unit area that is essential to decrease the interlayer distance by $\Delta R = (R_0 - R)$[9]

$$P = \frac{E - E_0}{\Delta R \times A} \quad (1)$$

where $E - E_0$ is the change in total energy in moving from strained to equilibrium configurations, A is the area of the unit cell, and ΔR ($R - R_0$) is the difference of the interlayer distance at strained and equilibrium configuration.

3.5. Carrier Mobilities. We apply a phonon-limited scattering model including the anisotropic characteristics of effective mass, elastic modulus, and DP to calculate room-temperature ($T = 300$ K) electron and hole mobilities using the formula[29,30]

$$\mu_{2D} = \frac{e\hbar^3 C_{2D}}{K_B T m^* m_a^* E_i^2} \quad (2)$$

DOI: 10.1021/acs.jpcc.8b08566
J. Phys. Chem. C XXXX, XXX, XXX−XXX

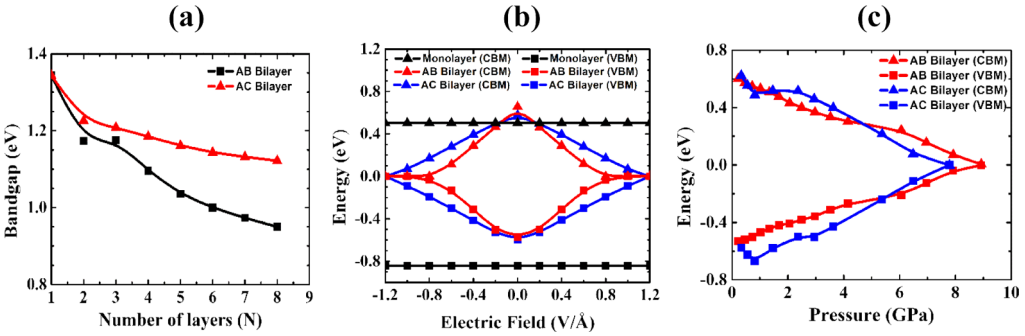

Figure 3. (a) Variation of band gap with number of layers, (b) variation of VBM and CBM with the applied perpendicular electric filed, and (c) variation of VBM and CBM with vertical pressure. In (b,c), zero is Fermi energy.

where, e is the electronic charge, $\hbar$ is the reduced Planck's constant, T is the temperature, k_B is the Boltzmann constant, and C_{2D} is in-plane elastic modulus in the propagation direction which is calculated using the formula

$$(E - E_0)/S_0 = C_{2D}(\Delta l/l_0)^2/2 \quad (3)$$

where $E - E_0$ represents the total energy change, S_0 is the area of the 2D cell, and $\Delta l/l_0$ is the deformation along x or y direction. m^* is the effective mass in the transport direction (i.e., either along x or y direction), and m_a^* is the average effective mass given by $\sqrt{m_x^* m_y^*}$. E_i in eq 2 is the DP constant calculated using the formula $E_i = \frac{dE_{edge}}{de}$ where E_{edge} is the energy of the CBM (VBM) for electrons (holes) and $e = \Delta l/l_0$.[31]

The carrier mobilities of 2D materials, which mostly govern their electronic properties, depend upon the carrier effective mass, elastic modulus, and the DP. It is found that the hole effective mass is highly anisotropic, whereas the electron effective mass remains almost isotropic for monolayer as well as AB- and AC-stacked bilayer green phosphorene. This behavior is similar to the one reported for black phosphorene in the literature.[31] The hole effective mass along the zigzag direction is 8.6, 8.4, and 8.0 times that along the armchair direction for monolayer and AB-stacked bilayer and AC-stacked bilayer green phosphorene, respectively [Table 2]. DP describes the change in energy of the electronic band with elastic deformation. A lower value of DP contributes to an increase in the mobility of electrons or holes. By including the anisotropic character of elastic constants [Table 1], effective mass, and DP, we estimate the carrier mobility of monolayer as well as bilayer green phosphorene using eq 2.

The electron mobilities are calculated to be higher than the hole mobilities of the monolayer as well as AB-stacked bilayer green-P, indicating their n-type behavior. AC-stacked bilayer green-P, on the other hand, behaves p-type along the armchair direction, whereas it shows n-type character along the zigzag direction. The order of magnitude of carrier mobilities (10 to 10^4 $cm^2/V/s$) reported in our calculations [Table 2] is comparable with black phosphorene.[31] The electron (hole) mobility anisotropy is calculated to be 19.7 (1.6), 2.3 (1.4), and 64.4 (68.5) for monolayer and AB-stacked bilayer and AC-stacked bilayer green phosphorene, respectively. Note that the mobility anisotropy is obtained as $R_a = \frac{\max(\mu_x, \mu_y)}{\min(\mu_x, \mu_y)}$, where $R_a = 1$ for isotropic systems and $R_a > 1$ for anisotropic systems.[37]

3.6. Strain Engineering in Monolayer and Bilayer Green Phosphorene: Potential Application in Photocatalytic Water Splitting. Considering the high carrier mobility of green phosphorene, we explore the feasibility to use green phosphorene for photocatalytic water splitting. Note that the material to act as a photocatalyst for water splitting requires its band gap to be at least 1.23 eV. Additionally, the CBM should be more positive than the redox potential of H_2/H^+ (0 V vs NHE) and the VBM should be more negative than the redox potential of H_2O/O_2.[38]

The overall process of water splitting is as follows

$$(\text{Green-P})^* \rightarrow h^+ + e^-$$

Oxidation (E vs NHE = 1.23 eV)

$$H_2O + 2h^+ \rightarrow 2H^+ + \frac{1}{2}O_2$$

Reduction (E vs NHE = 0 eV)

$$2H^+ + 2e^- \rightarrow H_2$$

Overall process

$$H_2O \xrightarrow{(\text{green-P})^*/h\nu} H_2 + \frac{1}{2}O_2$$

The mechanism of water splitting involves the excitation of electrons from the valence band to the conduction band of green phosphorene (monolayer and bilayer) by illuminating it with light of frequency greater than the band gap. Then, the holes in the valence band combines with the adsorbed water molecules to form H^+ and O_2 if their energy is greater than 1.23 eV (NHE). The H^+ produced combines with the electrons in the conduction band to form a H_2 molecule. Thus, the water molecule in the presence of green phosphorene (in the excited state) gets reduced to hydrogen and oxygen molecules. This is a general mechanism of water splitting and has been explained in various studies by performing oxidation and redox reactions of water on the surface of the photocatalyst.[39] In this paper, however, we mainly concentrated in exploring the possibility of modeling the band alignments and band gap of green phosphorene (monolayer and bilayer) by strain engineering or variation in the pH value to make green phosphorene a suitable candidate for water splitting.

We found that the band gap of monolayer green phosphorene is more than 1.23 eV. The tuning of band gap by applying mechanical strains can also be achieved in experimental situation.[40] Our calculations show that the

DOI: 10.1021/acs.jpcc.8b08566
J. Phys. Chem. C XXXX, XXX, XXX−XXX

change in band gap with in-plane uniaxial tensile and compression strain is highly anisotropic, which is attributed to the structural anisotropy of green phosphorene [Figure S3]. We found that the application of strain enables the band gap of AC-stacked bilayer green phosphorene to be greater than 1.23 eV. The change in VBM and CBM on application of strain is given in Figure 4. Maximum band gaps of 1.49 eV (1.37 eV)

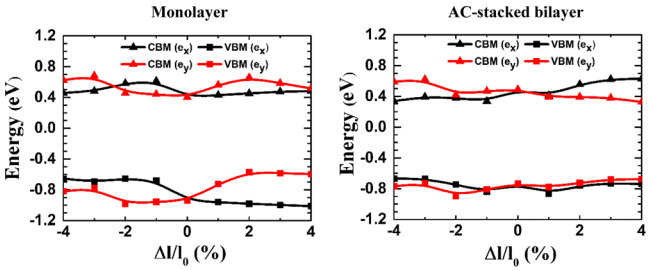

Figure 4. CBM and the VBM vs strain for monolayer and AC-stacked bilayer green phosphorene. Fermi energy plus vacuum energy are set to zero. For the monolayer, the band gap is highest at $\Delta x/x$ = 4% (band gap = 1.49 eV), $\Delta y/y$ = −3% (band gap = 1.46 eV), and for the AC-stacked bilayer, it is highest at $\Delta x/x$ = 4% (band gap = 1.37 eV), $\Delta y/y$ = −4% (band gap = 1.36 eV).

and 1.46 eV (1.36 eV) have been achieved in monolayer (AC-stacked bilayer) green phosphorene at uniaxial strain of 4% (4%) along x direction and −3% (−4%) along y direction, respectively.

For photocatalytic water splitting, not only the band gap should be appropriate but the band alignments should also match with the redox potential of water. It is found that the VBM in monolayer and AC-stacked bilayer green-P is less negative than the standard oxidation potential [Figure 5]. Therefore, as such, these systems cannot be used for water splitting. However, the standard redox potential depends on the pH of the solution. The standard oxidation potential H_2O/O_2 in a solution is given as[41]

$$E^{ox}_{O_2/H_2O} = 5.67\ \text{eV} - \text{pH} \times 0.059\ \text{eV}$$

Hence, the oxidation and redox potential will shift equally as the pH of the solution changes. We found that at pH = 14, the monolayer depicts favorable band positions to be used as a photocatalyst. Similarly, for uniaxial strain of +4% along x direction and for uniaxial strain of −3% along y direction, where the band gap reaches its maximum value, the favorable band alignment in the monolayer for photocatalysis is obtained for pH = 12 and pH = 14, respectively. Also, at pH values of 12 and 14, the band alignments of the 4% (along x direction) and −4% (along y direction) uniaxially strained AC-stacked bilayer (i.e., the strain values where its band gap value is maximum) become appropriate to be used as a catalyst for water splitting [Figure 5]. Thus, combining strain engineering with the pH of the solution, monolayer green-P and AC-stacked bilayer green-P can be potentially used for photocatalytic water splitting.

4. GREEN PHOSPHORENE/$MOSE_2$ HETEROSTRUCTURE: POTENTIAL APPLICATION IN PHOTOVOLTAICS

To be used in applications such as photovoltaics, the materials should be capable of absorbing broad solar spectra and must possess high carrier mobility. Our calculations show that optical absorption for monolayer as well as bilayer AB- and AC-stacked green phosphorene covers a wide range of solar spectrum, that is, from 1 to 4 eV which is significant for various applications based on solar energy [Figure S4].

To use bilayer green phosphorene in a thin-film photovoltaic system, an appropriate semiconducting acceptor material with matching band alignments must be found out. Specifically, it should form type II band alignments. Monolayer $MoSe_2$ has been found to exhibit the required band alignments for the acceptor material. This direct nature of the band gap [Figure 6] combined with high carrier mobility of monolayer and AB-

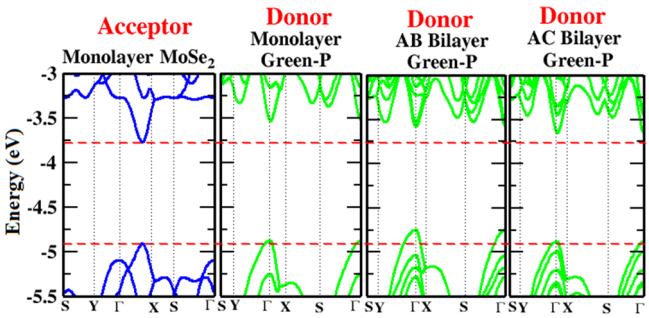

Figure 6. Electronic band structure of monolayer green phosphorene, AB- and AC-stacked bilayer green phosphorene, and monolayer $MoSe_2$. The red dashed lines in the band structures are drawn to indicate the band alignment of a green-phosphorene monolayer and bilayers with respect to monolayer $MoSe_2$. The vacuum level is set to be zero.

and AC-stacked bilayer green phosphorene indicates their potential to be used as a donor material for solar cell applications. The well-known that a $MoSe_2$ monolayer possesses a sandwich type of structure with a transition metal being sandwiched between the two layers of chalcogenides.[35] Note that the lattice mismatch between green phosphorene and monolayer $MoSe_2$ is less than 1% in

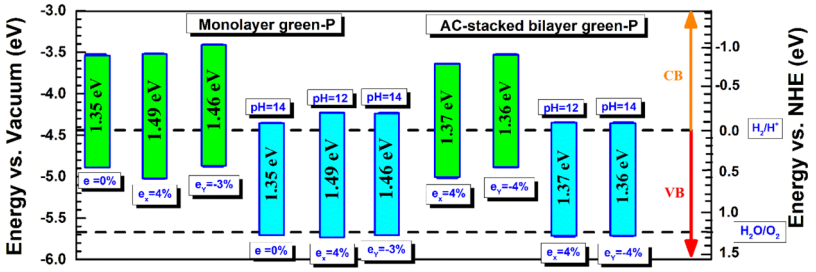

Figure 5. Energy alignment of monolayer and bilayer green phosphorene. Strain engineering and the pH value of the medium can modulate the band alignment. The green colored bars have zero pH value.

DOI: 10.1021/acs.jpcc.8b08566
J. Phys. Chem. C XXXX, XXX, XXX−XXX

both x- and y-direction [Figure S5]. In the limit of 100% external quantum efficiency (EQE), the upper limit to the PCE is calculated as follows[42,43]

$$\eta = \frac{J_{sc} V_{oc} \beta_{FF}}{P_{solar}} = \frac{0.65(E_g^d - \Delta E_c - 0.3)\int_{E_g}^{\infty} \frac{P(\hbar\omega)}{\hbar\omega} d(\hbar\omega)}{\int_{E_g}^{\infty} P(\hbar\omega)\, d(\hbar\omega)}$$

where 0.65 is the band fill factor, E_g^d is the band gap of the donor, and the term $(E_g^d - \Delta E_c - 0.3)$ estimates the maximum open-circuit voltage V_{oc}. $P(\hbar\omega)$ is the solar energy flux at air mass 1.5 (AM1.5) at photon energy $\hbar\omega$. The integral in the numerator depicts the short-circuit current J_{sc} in the limit of 100% EQE while the denominator is the solar energy flux at AM1.5.[44]

Our calculations show that the heterostructure constructed using monolayer and AB- and AC-stacked bilayer green phosphorene with $MoSe_2$ can achieve PCEs as high as 20, 18, and 21%, respectively [Figure 7]. These values are comparable

(a)

System	E_g (eV)	ΔE_C (eV)	PCE (%)
Monolayer green-P/$MoSe_2$	1.35	0.24	20
AB stacked green-P/$MoSe_2$	1.17	0.19	18
AC stacked green-P/$MoSe_2$	1.23	0.11	21

(b)

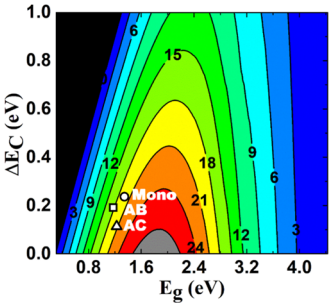

Figure 7. (a) Table for the band gap of the donor (E_g), conduction band offsets (ΔE_c), and percentage PCEs of the heterostructure of monolayer and AB- and AC-stacked bilayer green phosphorene with monolayer $MoSe_2$. (b) Calculated PCE contour as a function of donor band gap (E_g) and conduction band offsets (ΔE_c) of monolayer and AB- and AC-stacked bilayer green phosphorene with monolayer $MoSe_2$.

to those obtained for AA- and AB-stacked bilayer black phosphorene and MoS_2 (~18 and 16%),[24] α-AsP/GaN (~22.1%),[45] and PCBM/CBN systems (10−20%).[42] Note that the PCE value depends on E_g^d and ΔE_c.

5. SUMMARY

In summary, the electronic properties including the carrier mobility of the monolayer and bilayer green phosphorene are reported using state-of-the-art density functional theory. Semiconductor-to-metal transition has been found to be induced in bilayer systems through electric field, vertical pressure, and mechanical strain. Carrier mobilities are calculated to be highly anisotropic and stacking-dependent. Monolayer and AB-stacked bilayer green phosphorene possess n-type semiconducting behavior owing to their higher electron mobility. On the other hand, AC-stacked bilayer exhibits n-type and p-type character along armchair and zigzag directions, respectively. The high carrier mobility and sizable band gap of green phosphorene are important for the photovoltaics and water splitting photocatalysis. It is found that the strained monolayer and bilayer green phosphorene can be potential candidates for solar water splitting catalysis in highly basic medium. The upper limit to the PCEs of the monolayer and AB- and AC-stacked bilayer heterostructure with $MoSe_2$ are calculated to be comparable with the black phosphorene/MoS_2-based heterostructure. Hence, our results show the possibility of monolayer and bilayers of green phosphorene to be used in photovoltaic and photocatalytic applications.

■ ASSOCIATED CONTENT

Supporting Information

The Supporting Information is available free of charge on the ACS Publications website at DOI: 10.1021/acs.jpcc.8b08566.

Crystal structure of bulk green phosphorene, its band structure, and Brillioun zone; GGA-PBE lattice constant and bond lengths and layer thickness of a monolayer green phosphorene crystal structure; band gap versus strain for monolayer and AB-stacked and AC-stacked bilayer green phosphorene; computed imaginary part of the frequency-dependent dielectric function; and heterostructures of AB-stacked bilayer green phosphorene with $MoSe_2$ and AC-stacked bilayer green phosphorene with $MoSe_2$ (PDF)

■ AUTHOR INFORMATION

Corresponding Authors

*E-mail: ashokphy@cup.edu.in (A.K.).
*E-mail: sunita@pu.ac.in (S.S.).
*E-mail: tkumar@gjust.org (K.T.).

ORCID

Ashok Kumar: 0000-0003-3636-0502

Notes

The authors declare no competing financial interest.

■ ACKNOWLEDGMENTS

S.K. is grateful to UGC-BSR for financial assistance in the form of senior research fellowship. A.K. gratefully acknowledges University Grants Commission for Start-up grants [30-318/2016 (BSR)]. The computational facility at Central University of Punjab, Bathinda, and RAMA High-Performance Computing Cluster at Michigan Technological University Houghton, USA, are used to obtain the results presented in this paper.

■ REFERENCES

(1) Brent, J. R.; Savjani, N.; Lewis, E. A.; Haigh, S. J.; Lewis, D. J.; O'Brien, P. Production of few-layered phosphorene by liquid exfoliation of black phosphorous. *Chem. Commun.* **2014**, *50*, 13338−13341.

(2) Das, S.; Zhang, W.; Demarteau, M.; Hoffmann, A.; Dubey, M.; Roelofs, A. Tunable Transport Gap in Phosphorene. *Nano Lett.* **2014**, *14*, 5733−5739.

(3) Gusmão, R.; Sofer, Z.; Pumera, M. Black Phosphorus Rediscovered: From Bulk to Monolayer. *Angew. Chem., Int. Ed.* **2017**, *56*, 8052−8072.

(4) Sorkin, V.; Cai, Y.; Ong, Z.; Zhang, G.; Zhang, Y. W. Recent Advances in the Study of Phosphorene and its Nanostructure. *Crit. Rev. Solid State Mater. Sci.* **2017**, *42*, 1−82.

(5) Carvalho, A.; Wang, M.; Zhu, X.; Rodin, A. S.; Su, H.; Neto, A. H. C. Phosphorene: from theory to applications. *Nat. Rev. Mater.* **2016**, *11*, 16061.

(6) Liu, H.; Neal, A. T.; Zhu, Z.; Luo, Z.; Xu, X.; Tománek, D.; Ye, P. D. Phosphorene: An Unexplored 2D Semiconductor with a High Hole Mobility. *ACS Nano* **2014**, *8*, 4033−4041.

(7) Xiao, J.; Long, M.; Zhang, X.; Ouyang, J.; Xu, H.; Gao, Y. Theoretical predictions on the electronic structure and charge carrier mobility in 2D Phosphorus sheets. *Sci. Rep.* **2015**, *5*, 9961.

DOI: 10.1021/acs.jpcc.8b08566
J. Phys. Chem. C XXXX, XXX, XXX−XXX

(8) Shu, H.; Li, Y.; Niu, X.; Wang, J. The stacking dependent electronic structure and optical properties of bilayer black phosphorus. *Phys. Chem. Chem. Phys.* **2016**, *18*, 6085−6091.
(9) Kaur, S.; Kumar, A.; Srivastava, S.; Tankeshwar, K. Electronic structure engineering of various structural phases of phosphorene. *Phys. Chem. Chem. Phys.* **2016**, *18*, 18312−18322.
(10) Guan, J.; Zhu, Z.; Tománek, D. Phase coexistence and metal insulator transition in few-layer phosphorene: A computational study. *Phys. Rev. Lett.* **2014**, *113*, 046804.
(11) Wu, M.; Fu, H.; Zhou, L.; Yao, K.; Zeng, X. C. Nine New Phosphorene Polymorphs with Non-Honeycomb Structures: A Much Extended Family. *Nano Lett.* **2015**, *15*, 3557−3562.
(12) Wang, H.; Li, X.; Liu, Z.; Yang, J. *ψ*-phosphorene: a new allotrope of phosphorene. *Phys. Chem. Chem. Phys.* **2017**, *19*, 2402.
(13) Zhao, T.; He, C. Y.; Ma, S. Y.; Zhang, K. W.; Peng, X. Y.; Xie, G. F.; Zhong, J. X. A new phase of phosphorus: the missed tricycle type red phosphorene. *J. Phys.: Condens. Matter* **2015**, *27*, 265301.
(14) Zhang, Y.; Wu, Z.-F.; Gao, P.-F.; Fang, D.-Q.; Zhang, E.-H.; Zhang, S.-L. Structural, elastic, electronic, and optical properties of the tricycle-like phosphorene. *Phys. Chem. Chem. Phys.* **2017**, *19*, 2245−2251.
(15) Li, P.; Luo, W. A new structure of two-dimensional allotropes of group V elements. *Sci. Rep.* **2016**, *6*, 25423.
(16) Xu, M.; He, C.; Zhang, C.; Tang, C.; Zhong, J. First-principles prediction of a novel hexagonal phosphorene allotrope. *Phys. Status Solidi RRL* **2016**, *10*, 563−565.
(17) Kaur, S.; Kumar, A.; Srivastava, S.; Pandey, R.; Tankeshwar, K. Stability and carrier transport properties of phosphorene-based polymorphic nanoribbons. *Nanotechnology* **2018**, *29*, 155701.
(18) Qiu, M.; Sun, Z. T.; Sang, D. K.; Han, X. G.; Zhang, H.; Niu, C. M. Current progress in black phosphorus materials and their applications in electrochemical energy storage. *Nanoscale* **2017**, *9*, 13384−13403.
(19) Zhang, J. L.; Zhao, S.; Han, C.; Wang, Z.; Zhong, S.; Sun, S.; Guo, R.; et al. Epitaxial growth of single layer blue phosphorus: a new phase of two-dimensional phosphorus. *Nano Lett.* **2016**, *16*, 4903−4908.
(20) Xu, J.-P.; Zhang, J.-Q.; Tian, H.; Xu, H.; Ho, W.; Xie, M. One-dimensional phosphorus chain and two-dimensional blue phosphorene grown on Au (111) by molecular-beam epitaxy. *Phys. Rev. Mater.* **2017**, *1*, 061002.
(21) Zeng, J.; Cui, P.; Zhang, Z. Half Layer By Half Layer Growth of a Blue Phosphorene Monolayer on a GaN (001) Substrate. *Phys. Rev. Lett.* **2017**, *118*, 046101.
(22) Han, W. H.; Kim, S.; Lee, I.-H.; Chang, K. J. Prediction of Green Phosphorus with Tunable Direct Band Gap and High Mobility. *J. Phys. Chem. Lett.* **2017**, *8*, 4627−4632.
(23) Yang, G.; Ma, T.; Peng, X. Superior mechanical flexibility and strained-engineered direct-indirect band gap transition of green phosphorene. *Appl. Phys. Lett.* **2018**, *112*, 241904.
(24) Dai, J.; Zeng, X. C. Bilayer phosphorene: effect of stacking order on bandgap and its potential applications in thin-film solar cells. *J. Phys. Chem. Lett.* **2014**, *5*, 1289−1293.
(25) Lu, N.; Guo, H.; Wang, L.; Wu, X.; Zeng, X. C. Van der Waals trilayers and superlattices: modification of electronic structures of MoS_2 by intercalation. *Nanoscale* **2014**, *6*, 4566−4571.
(26) Soler, J. M.; Artacho, E.; Gale, J. D.; García, A.; Junquera, J.; Ordejón, P.; Sánchez-Portal, D. The SIESTA method for ab initio order-N Materials Simulation. *J. Phys.: Condens. Matter* **2002**, *14*, 2745−2779.
(27) Troullier, N.; Martins, J. L. Efficient Pseudopotentials for Plane-Wave Calculations. *Phys. Rev. B: Condens. Matter Mater. Phys.* **1991**, *43*, 1993−2006.
(28) Dion, M.; Rydberg, H.; Schröder, E.; Langreth, D. C.; Lundqvist, B. L. van der Waals Density Functional for General Geometries. *Phys. Rev. Lett.* **2004**, *92*, 246401.
(29) Bardeen, J.; Shockley, W. Deformation Potentials and Mobilities in Non-Polar Crystals. *Phys. Rev.* **1950**, *80*, 72.
(30) Xie, J.; Zhang, Z. Y.; Yang, D. Z.; Si, M. S.; Xue, D. S. A large enhancement of carrier mobility in phosphorene by introducing hexagonal boron nitride substrate. **2016**, arXiv preprint arXiv:1610.03185.
(31) Qiao, J.; Kong, X.; Hu, Z.-X.; Yang, F.; Ji, W. High-mobility transport anisotropy and linear dichroism in few-layer black phosphorus. *Nat. Commun.* **2014**, *5*, 4475.
(32) Peng, X.; Wei, Q.; Copple, A. Strain-engineered direct-indirect band gap transition and its mechanism in two-dimensional phosphorene. *Phys. Rev. B: Condens. Matter Mater. Phys.* **2014**, *90*, 085402.
(33) Kumar, A.; Ahluwalia, P. K. Mechanical strain dependent electronic and dielectric properties of two-dimensional honeycomb structures of MoX2 (X= S, Se, Te). *Phys. B* **2013**, *419*, 66−75.
(34) Swaroop, R.; Ahluwalia, P. K.; Tankeshwar, K.; Kumar, A. Ultra-narrow blue phosphorene nanoribbons for tunable optoelectronics. *RSC Adv.* **2017**, *7*, 2992−3002.
(35) Kaur, S.; Kumar, A.; Srivastava, S.; Tankeshwar, K. van der Waals heterostructures based on allotropes of phosphorene and $MoSe_2$. *Phys. Chem. Chem. Phys.* **2017**, *19*, 22023−22032.
(36) Kumar, A.; Ahluwalia, P. K. Electronic structure of transition metal dichalcogenides monolayers 1H-MX 2 (M= Mo, W; X= S, Se, Te) from ab-initio theory: new direct band gap semiconductors. *Eur. Phys. J. B* **2012**, *85*, 186.
(37) Lang, H.; Zhang, S.; Liu, Z. Mobility anisotropy of two-dimensional semiconductors. *Phys. Rev. B: Condens. Matter Mater. Phys.* **2016**, *94*, 235306.
(38) Gupta, U.; Rao, C. N. R. Hydrogen generation by water splitting using MoS 2 and other transition metal dichalcogenides. *Nano Energy* **2017**, *41*, 49−65.
(39) Lv, X.; Wei, W.; Sun, Q.; Li, F.; Huang, B.; Dai, Y. Two-dimensional germanium monochalcogenides for photocatalytic water splitting with high carrier mobility. *Appl. Catal., B* **2017**, *217*, 275−284.
(40) Feng, J.; Qian, X.; Huang, C.-W.; Li, J. Strain-engineered artificial atom as a broad-spectrum solar energy funnel. *Nat. Photonics* **2012**, *6*, 866−872.
(41) Sa, B.; Li, Y.-L.; Qi, J.; Ahuja, R.; Sun, Z. Strain engineering for phosphorene: the potential application as a photocatalyst. *J. Phys. Chem. C* **2014**, *118*, 26560−26568.
(42) Bernardi, M.; Palummo, M.; Grossman, J. C. Semiconducting monolayer materials as a tunable platform for excitonic solar cells. *ACS Nano* **2012**, *6*, 10082−10089.
(43) Zhou, L.-J.; Zhang, Y.-F.; Wu, L.-M. SiC2 siligraphene and nanotubes: novel donor materials in excitonic solar cells. *Nano Lett.* **2013**, *13*, 5431−5436.
(44) The AM1.5G spectrum was taken from the NREL website: http://rredc.nrel.gov/solar/spectra/am1.5/ASTMG173/ASTMG173.html.
(45) Xie, M.; Zhang, S.; Cai, B.; Huang, Y.; Zou, Y.; Guo, B.; Gu, Y.; Zeng, H. A promising two-dimensional solar cell donor: Black arsenic−phosphorus monolayer with 1.54 eV direct bandgap and mobility exceeding 14,000 cm $^2V^{-1}$ s^{-1}. *Nano Energy* **2016**, *28*, 433−439.

DOI: 10.1021/acs.jpcc.8b08566
J. Phys. Chem. C XXXX, XXX, XXX−XXX